


Intracellular protons accelerate aging and switch on aging hallmarks in mice

Tomohiro Osanai MD¹  | Makoto Tanaka MD² | Kei Izumiyama MD³ | Kasumi Mikami RN PhD¹ | Maiko Kitajima RN PhD¹ | Toshiko Tomisawa RN PhD¹ | Koji Magota PhD⁴ | Hirofumi Tomita MD³ | Ken Okumura MD⁵

¹Department of Nursing Science, Hirosaki University Graduate School of Health Science, Hirosaki, Japan

²Department of Hypertension and Stroke Internal Medicine, Hirosaki University Graduate School of Medicine, Hirosaki, Japan

³Department of Cardiology, Hirosaki University Graduate School of Medicine, Hirosaki, Japan

⁴Daiichi Sankyo Co, Ltd, Biologics Technology Research Laboratories Group 1, Pharmaceutical Technology Division, Gunma, Japan

⁵Saiseikai Kumamoto Hospital, Division of Cardiology, Kumamoto, Japan

Correspondence

Tomohiro Osanai, MD, Department of Nursing Science, Hirosaki University Graduate School of Health Science, 66-1 Hon-cho, Hirosaki 036-8564, Japan. Email: osanait@hirosaki-u.ac.jp

Funding information

Grant-in-Aid for Scientific Research, Grant/Award Numbers: 19590800, 15K09151, 21590946; Ministry of Education, Culture, Sports, Science and Technology, Japan

Abstract

Diet-induced metabolic acidosis is associated with the impairment of bone metabolism and an increased risk of a number of chronic noncommunicable diseases, such as type 2 diabetes mellitus and hypertension. The serum bicarbonate level is an independent predictor of chronic kidney disease progression. We investigated whether proton accelerates aging by analyzing both coupling factor 6-overexpressing transgenic (TG) and high salt-fed mice which display sustained intracellular acidosis, due to enhanced proton import through ecto-F₁F_o complex and/or reduced proton export through Na⁺-K⁺ ATPase inhibition. Both types of mice displayed shortened lifespan and early senescence-associated phenotypes such as signs of hair greying and alopecia, weight loss, and/or reduced organ mass. In chronic intracellular acidosis mice, autophagy was impaired by regression of Atg7, an increase in nuclear acetylated LC3 II, and acetylation of Atg7. The increase in histone 3 trimethylation at lysine 4 (H3K4me3) and H4K20me3 and the decrease in H3K9me3 and H3K27me3 were observed in the heart and kidney obtained from both TG and high salt-fed mice. The decrease in lamin A/C, emerin, and heterochromatin protein 1 α without changes in barrier-to-autointegration factor and high-mobility group box 1 was confirmed in TG and high salt-fed mice. Suppression of nuclear histone deacetylase 3-emerin system is attributable to epigenetic regression of Atg7 and H4K5 acetylation. These findings will shed light on novel aging and impaired autophagy mechanism, and provide implications in a target for antiaging therapy.

KEYWORDS

aging, ATP synthase, autophagy, coupling factor 6, epigenetics, genomic instability, intracellular acidosis, salt

1 | INTRODUCTION

Aging is characterized by a progressive loss of physiological integrity. A number of factors contribute to the aging process and phenotype.¹ Cellular senescence, reactive oxygen

species, and optimal nutrient sensing accelerate aging at high levels, but mediate beneficial effects at low levels, indicating usefulness of caloric restriction² and removal of senescent cells³ as antiaging therapy. In contrast, genomic instability, telomere attrition, epigenetic alterations, and

defective proteostasis are the initiating triggers whose damaging events accumulate with time.¹

The oxidative stress theory of aging is based on the hypothesis that age-associated functional losses are due to the accumulation of reactive oxygen species-induced damages. At the same time, oxidative stress is involved in several age-related conditions such as cardiovascular diseases, chronic obstructive pulmonary disease, chronic kidney disease, neurodegenerative diseases, and cancer. Given the important role of oxidative stress in the pathogenesis of many clinical conditions and aging, antioxidant therapy could positively affect the natural history of several diseases.⁴ On the other hand, cellular senescence participates in four complex biological processes such as tumor suppression, tumor promotion, aging, and tissue repair, some of which have apparently opposing effects.⁵

Diet-induced metabolic acidosis has been reported to be associated with the impairment of bone metabolism and an increased risk of a number of chronic noncommunicable diseases, such as type 2 diabetes mellitus and hypertension.⁶⁻⁸ Low serum bicarbonate is associated with high mortality in healthy older individuals.⁹ Proton regulates cellular function by modulating the charge and structure of macromolecules. Therefore, it is likely that intracellular protons orchestrate aging hallmarks and accelerate aging with shortened lifespan. We recently identified coupling factor 6 (CF6) as a novel ligand for ecto-F₁F_o complex, and after binding to protrusive F₁, CF6 forces the backward rotation of F_o, thereby stimulating proton import at the plasma membrane.¹⁰ In the plasma membrane, F₁ can hydrolyze ATP and inversely rotate F_o to pump protons in the opposite direction when the free energy of ATP hydrolysis is large in the extracellular space, leading to intracellular acidosis. CF6 has been disclosed to exert a widespread action of vascular biology such as inhibition of prostacyclin and platelet endothelial cell adhesion molecule 1, and stimulation of endogenous nitric oxide synthases inhibitor asymmetric dimethyl arginine.¹¹⁻¹⁷ In the clinical settings, we and others showed that circulating CF6 is elevated in patients with end-stage renal disease, myocardial infarction, stroke, hypertension, and diabetes,¹⁸⁻²¹ all of which are aging-related diseases. Based on these backgrounds, we examined whether or not proton accelerates aging by analyzing CF6-overexpressing transgenic (TG) and high salt-fed mice which display sustained intracellular acidosis. In the current study, we show that protons accelerate aging and switch on aging hallmarks regardless of whether ischemic hypoxia and/or kidney dysfunction are absent or present.

2 | MATERIALS AND METHODS

2.1 | Materials

Effectene Transfection Reagent, QIA shredder, and RNeasy Protect Mini Kit were from Qiagen (Valencia, CA). Gibco Dulbecco modified Eagle medium (DMEM), fetal bovine serum (FBS), and penicillin/streptomycin were from Life Technology Corporation (Tokyo, Japan). Amino Allyl MessageAmp aRNA kit was from Ambion (Foster City, CA). RIPA lysis buffer, antibody for GAPDH, and mouse monoclonal antibody for emerlin were from Santa Cruz Biotechnology (Santa Cruz, CA). Antibodies for human histone deacetylase 1 to 4 (HDAC1-4), acetyl-histone 4 at lysine 5 (H4K5), and trimethylation of H3K4, K9, K27, and H4K20, lamin A/C, heterochromatin protein 1 α (HP1 α), p62, and Atg7 were from Cell Signaling Technology, Inc (Danvers, MA). Antibodies for pan-acetyl histone 3 and 4 were from Active Motif Inc (Tokyo, Japan). Mouse monoclonal antibody for LC3 was from Cosmo Bio Co, Ltd (Tokyo, Japan). Rabbit polyclonal antibody for Lamp 1 was from Abcam (Tokyo, Japan). ReadyPrep protein extraction kit (cytoplasmic/nuclear) was from Bio-Rad Laboratories, Inc (Hercules, CA). TransIT-293 Transfection Reagent was from Mirus Bio LLC (Madison, WI). AceGene-Mouse Oligo Chip 30K 1 Chip version was from Hitachi Software Engineering Co, Ltd (Kanagawa, Japan). Cy3-conjugated or Cy5-conjugated deoxyribonucleotides were from Amersham Biosciences (Freiburg, Germany). ³H-water was from New England Nuclear (Boston, MA). Polyvinylidene difluoride membrane was from Bio-Rad Laboratories. Enhanced chemiluminescence plus detection systems were from Amersham Pharmacia Biotech (Piscataway, NJ). All other reagents were of the finest grade available from Sigma Chemical Co (St Louis, MO).

2.2 | Construction of vectors and generation of CF6-overexpressing TG mice

The mature ATP synthase CF6 (Asn 33 to Ala 108) gene was subcloned into pNE plasmid, in which β -globin promoter of pdKCR-dhfr plasmid were replaced by human elongation factor-1 α promoter. The resultant recombinant plasmid was digested with PvuII and Aor51HI to generate 2.8 kb of DNA fragment consisting of the human elongation factor 1 α promoter, secretion signal/CF6-fused gene and SV40 polyA additional sequence. The DNA fragment was then microinjected into the pronuclei of single cell-fertilized mouse embryos to generate TG mice. It was confirmed in the study by using COS cells that the expressed protein was released outside of the cells as the form of mature

human CF6 (Asn33 to Ala108). CF6-TG mice and wild type (WT) littermate mice C57BL/6J were maintained with standard rat chow and free access to water. The animal's care was in accordance with institutional guidelines. The protocol of the current study was approved by the ethics committee of the Hirosaki University Graduate School of Medicine.

2.3 | Diet and lifespan study

Mice were fed a normal salt diet until the age of 11 weeks, and were followed by a high salt diet (8% salt; Oriental Yeast, Tokyo, Japan) or by a normal salt diet continuously. A prospective observational study was performed in 20 homozygous TG mice and 20 WT littermate controls, both of which were fed a normal or high salt diet.

2.4 | Blood pressure measurement

Systolic and diastolic arterial blood pressures were measured by tail-cuff method in conscious mice by using the Softron BP-98A system (Softron Co, Tokyo, Japan). Blood pressures were measured 10 times per day for 4 consecutive days, and a mean value was generated for each individual mouse.

2.5 | Measurement of intracellular pH

³¹P-magnetic resonance spectroscopy (MRS) of the femoral skeletal muscle and the liver was performed by using the 4.7-T JASTEC horizontal magnet with the mouse in a supine position and a 20-mm-diameter surface coil under the muscle and the liver. Spectra were acquired using a 0.5-second repetition time and 50 μs pulse width. Relative concentrations of inorganic phosphate and PCr were obtained using a time-domain fitting routine and were corrected for partial saturation. Intracellular pH was calculated from the chemical shift of the Pi peak relative to PCr (δPi; measured in parts per million, ppm), using the equation: $\text{pH} = 6.75 + \log\left(\frac{\delta\text{Pi} - 3.27}{5.69 - \delta\text{Pi}}\right)$.

2.6 | Measurement of ³H uptake

³H-water (0.01 MBq/g body weight in 200 μL of phosphate buffered saline [PBS]; New England Nuclear) was injected into the peritoneal cavity under anesthesia (ketamine at 75 mg/kg and xylazine at 7.5 mg/kg), and the [³H] level after 15 minutes in each tissue was counted with a liquid scintillation counter.

2.7 | Cell culture

Primary mouse cardiac fibroblasts from CF6-overexpressing mice and WT mice and HEK-293 cells were cultured in DMEM supplemented with 10% FBS, 100 U/mL of penicillin, and 100 μg/mL of streptomycin at 37°C under 5% CO₂. Fibroblasts from the second to seventh passages were used.

2.8 | RNA isolation

The tissues and cells were rinsed quickly in ice-cold PBS and RNA was isolated by using RNeasy Mini Kit (QIAGEN, Venlo, Netherland) according to the manufacturer's instructions. RNA quality was insured by spectrophotometric analysis (OD_{260/280}). The RNA was quantitated by spectrophotometric analysis at 260 nm. Linear amplification of messenger RNA from total RNA was obtained using the Amino Alkyl MessageAmp aRNA Kit (Thermo Fisher Scientific Inc., Tokyo, Japan) with two consecutive amplification steps according to the manufacturer's recommendations. Two replicates of each experiment were carried out using different microarray slides where the RNA samples from two different sources were labelled with either Cy3-conjugated or Cy5-conjugated deoxyribonucleotides. The fluorescent dye on probes derived from the experimental aRNA was Cy5, while the dye on control probes was Cy3.

2.9 | cDNA microarrays

We used a commercially available complementary DNA (cDNA) microarray, the AceGene-Mouse Oligo Chip 30K 1 Chip version, which contained 30 000 cDNA named mouse genes, to identify genes altered in the heart and kidney either between TG and WT mice or high salt intake. Labeled probes were mixed with a hybridization solution (5× sodium chloride and sodium citrate [SSC], 0.5% sodium dodecyl sulfate [SDS], 4× Denhardt solution, 20% hybridization solution, 0.1 mg/mL of denatured salmon sperm DNA, and 10% formamide). After hybridization for 14 hours at 46°C, the slides were washed in 5× SSC and 0.1% SDS for 2 minutes at room temperature, 5× SSC and 0.1% SDS for 10 minutes at 30°C, 0.5× SSC for 2 minutes at room temperature. Slides were scanned for Cy3 and Cy5 fluorescence with a 428 ARRAY scanner (Affymetrix, Tokyo, Japan), and the fluorescence was quantified with DNASIS Array software version 2.6 (Hitachi Software Engineering Co, Ltd). The current analysis used intensity dependent Global Normalization (mean: 10 000). Intensity-dependent normalization is just one technique used to eliminate dye-related artifacts in two-color experiments such as this. The results for each gene were reported as an average obtained from three slides. The data are reported as

the normalized ratio of Cy5 (for CF6+) to Cy3 (for CF6-). We used intensity of 2000 or above.

2.10 | Determination of protein expression

Tissue and cell samples were homogenized in RIPA lysis buffer (20 mmol/L of Tris-HCl, pH 7.5, 150 mmol/L of NaCl, 1 mmol/L of EDTA, 1 mmol/L of EGTA, 1% Triton X-100, 1% glycerol, 1 mmol/L of dithiothreitol, and 0.5 mmol/L of phenylmethylsulfonyl fluoride). Samples were mixed with Laemelli buffer that contained 5% β -mercaptoethanol and were loaded onto SDS-polyacrylamide gel electrophoresis. Protein was transferred electrophoretically to a polyvinylidene difluoride membrane, and

was incubated with the primary antibodies for LC3II, p62, Atg7, HHAC1 to 4, pan-acetyl H3, pan-acetyl H4, H4K5, H3K4me3, H3K9me3, H3K27me3, H4K20me3, emerlin, lamin A/C, HP1 α , and GAPDH at 4°C overnight. The protein bands were detected by the enhanced chemiluminescence plus detection systems. Densitometric analysis was performed with Scion image software, and the relative ratio to the protein bands was calculated in each sample. The band detection was all within the linear range.

2.11 | Histological analysis

Histological analysis was performed by fixing skin overnight in 10% phosphate-buffered formalin and

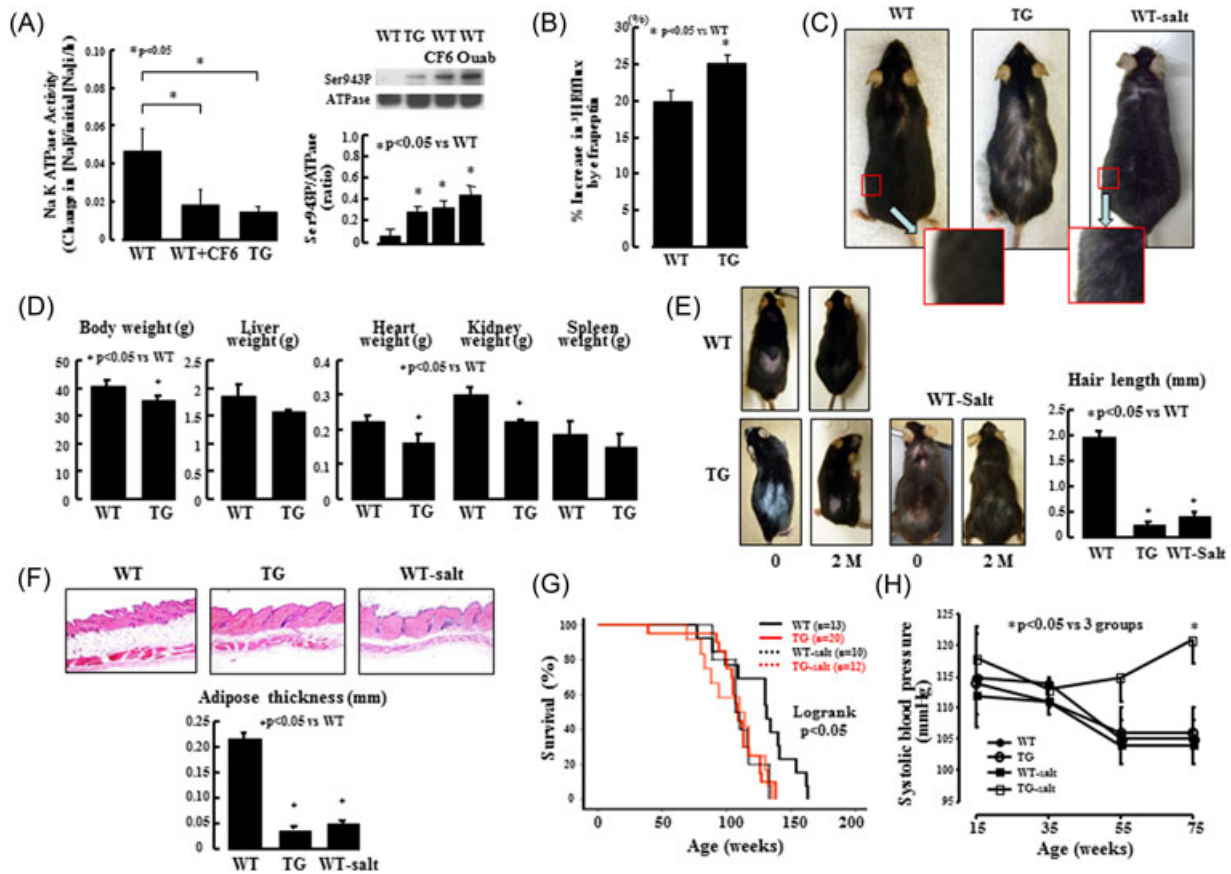


FIGURE 1 Accelerated aging phenotype in coupling factor 6 (CF6) overexpressing transgenic mice (TG) and high salt-fed mice. A, Na⁺-K⁺-ATPase activity in wild type (WT) cells treated with or without CF6 at 10⁻⁷ M for 2.5 hours and TG cells (n = 5, respectively) in 10% FBS-DMEM. Phosphorylation of α subunit of Na⁺-K⁺-ATPase at serine 943 in WT cells treated with or without CF6 at 10⁻⁷ M or ouabain at 10⁻⁶ M and TG cells. Either CF6 or ouabain relating to salt sensitivity phosphorylated α subunit of Na⁺-K⁺-ATPase at serine 943 to inhibit its activity in cultured fibroblasts (n = 3). Representative bands were shown. B, Percent inhibition of ³H excretion rate for 8 minutes by efrapreptin at 10⁻⁵ M in skeletal muscle from WT and TG mice (n = 4, respectively). TG displayed reduced proton excretion in skeletal muscle ex vivo. C, Representative hair conditions of WT, TG, and high salt-fed WT mice at the age of 100 weeks. D, Organ weights in 100-week-old TG and WT mice (n = 12, respectively). E, Hair growth phenotypes in TG, WT, and high salt-fed WT mice. Representative 100-week-old mice before and 2 months after removal of hair from a 2-cm² dorsal area. Similar results were obtained in separate four experiments. F, Cross-sections of dorsal skin from 100-week-old TG, WT, and high salt-fed WT mice (n = 7, respectively). G, Survival curve of normal or high salt-fed TG and WT mice (n = 10 to 20). H, Systolic blood pressure in normal or high salt-fed TG and WT mice (n = 10 to 20). DMEM, Dulbecco modified Eagle medium; FBS, fetal bovine serum

processed into paraffin blocks for section. Serial-5 μm sections were stained with hematoxylin and eosin.

2.12 | Statistical analysis and ethical considerations

Results were expressed as mean \pm SEM. Differences between groups were examined for statistical significance using Student *t* test or analysis of variance with Bonferroni test.

3 | RESULTS

3.1 | How can CF6 and salt induce sustained intracellular acidosis?

While searching endogenous inhibitors of prostacyclin synthesis, we identified 76-amino acid peptide CF6, which is localized at the stalk of mitochondrial F_1F_0 complex and a novel ligand for plasma membrane ecto- F_1F_0 complex. After binding to protrusive F_1 at the plasma membrane, CF6 stimulates proton import by forcing the backward rotation of F_0 ,¹⁰ and inhibits three proton extruders, $\text{Na}^+\text{-H}^+$ exchanger, $\text{Na}^+\text{-HCO}_3^-$ co-transporter, and Na^+ -dependent $\text{Cl}^-\text{-HCO}_3^-$ exchanger by decreasing the inwardly directed electrochemical Na^+ gradient, which is created by $\text{Na}^+\text{-K}^+\text{-ATPase}$ pump.²² Because phosphorylation of α subunit of $\text{Na}^+\text{-K}^+\text{-ATPase}$ at serine 943 resulted in the suppression of its activity,²³ we examined whether CF6 and ouabain phosphorylates α subunit of $\text{Na}^+\text{-K}^+\text{-ATPase}$ at serine 943. As shown in Figure 1A, CF6 and ouabain phosphorylated α subunit of $\text{Na}^+\text{-K}^+\text{-ATPase}$ at serine 943 and inhibited its activity in cultured fibroblasts. Regardless of an aerobic condition, therefore, TG displayed reduced proton excretion from skeletal muscle, which is assessed by *ex vivo* measurement of ^3H excretion rate (Figure 1B). More direct *in vivo* measurement by ^{31}P -MRS demonstrated that TG liver displayed the decrease in intracellular pH ranging from 0.1 to 0.15 U compared with WT mice,¹⁶ and the pH value of the liver was similar between TG and high salt-fed mice at 51 to 89 weeks age (pH 7.25 ± 0.02 U in salt-fed WT vs 7.26 ± 0.03 U in TG, $P = \text{ns}$).

3.2 | Sustained intracellular acidosis accelerates aging phenotype and shortens lifespan

We characterized the aging-related phenotypes early in life in TG or high salt-fed mice. Up to 75 weeks of age, TG mice appeared morphologically identical to their WT littermates; however, at the age of 100 weeks, most of the TG mice manifested the early aging-related phenotype such as signs of hair greying and alopecia, weight loss,

and reduced organ mass (Figure 1C and 1D). The hair in the older TG mice was sparser than that of their WT counterparts, and hair greying was more frequent in TG mice than in WT mice. Like TG mice, high salt-fed mice showed hair greying and alopecia compared with normal salt-fed WT mice (Figure 1C, arrow). In a hair-growth assay which involves shaving a dorsal segment of skin in the mouse and measuring the amount of hair growth after 2 months, little hair growth was observed in TG and high salt-fed mice compared with age-matched WT mice (Figure 1E). Histological cross-sections of dorsal skin revealed wrinkly dermal tissues and significant reductions in mean subcutaneous adipose thickness in TG and high salt-fed mice (Figure 1F).

Consistent with accelerated aging, TG mice were short-lived compared with WT mice (median values; 108 ± 2 vs 131 ± 11 weeks, $P < 0.05$) (Figure 1G) and no difference was found between gender (Supporting Information Figure S1). At 138 weeks, while all TG mice died, 38% of WT mice were still alive, and these lived for an additional 25-week period (the maximal lifespan of WT mice, 163 weeks). We further analyzed the effect of high salt intake on lifespan while monitoring arterial blood pressure. Under high salt diet, lifespan was shortened to 107 ± 8 and 110 ± 17 weeks of the median values and 133 and 135 weeks of the maximal lifespan in WT and TG mice, respectively (both $P < 0.05$ vs normal salt-fed WT mice, by log rank test). Besides 10 mm Hg elevation of systolic blood pressure (Figure 1H), no physiological parameters were influenced by high salt diet in TG mice (Supporting Information Figure S2).

3.3 | Identification of a key molecule for accelerated aging and impaired autophagy

To characterize aging hallmarks which accelerate aging and shorten lifespan in TG and high salt-fed mice, we measured autophagy-related proteins in the heart and kidney of TG and high salt-fed mice by Western blot analysis. The increase in LC3 II and P62 was confirmed in TG heart and liver besides the kidney (Figure 2A). Tissue preparation with acidosis or amiloride at 10^{-4} M induced the increase in LC3 II and P62 in the heart and liver (Figure 2B). As shown in Figure 2C, Atg7 protein was decreased in the heart, kidney, and liver in TG and high salt-fed WT mice. Furthermore, acetylation of Atg7 which inhibits autophagy was increased in the TG heart and kidney (Figure 2D). Overall, the higher expression of LC3 II and P62, which shows chronic impaired autophagy, is due to the decrease in Atg7 and the increase in nuclear-acetylated LC3 II. In addition, acetylation of Atg7 might further exaggerate impaired autophagy.

3.4 | Aging-related epigenetic alterations in TG and high salt-fed mice

We investigated impact of sustained intracellular acidosis on aging epigenetic markers such as global hypomethylated DNA, increased H4K16ac, H4K20me3, or H3K4me3 as well as decreased H3K9me3 or H3K27me3.¹ These markers transmit as epigenetic memory, and demethylation of H3K4me3 extends lifespan in nematodes.²⁴ The de novo DNA methyltransferase (Dnmt3b) was decreased in TG and high salt-fed mice despite no changes in the maintenance DNA methyltransferase (Dnmt1) and its modulator ubiquitin like with PHD and ring finger domains 1 (Uhrf1), suggesting that global hypomethylated DNA may be present in our models and cause genomic instability (Table 1).

As shown in Figure 3A, the increase in H3K4me3 and H4K20me3 and the decrease in H3K9me3 and H3K27me3 were observed in the heart and kidney obtained from both TG and high salt-fed mice. Independent of methyltransferases Ash-2 or Suv420h1 to 2, the decrease in histone demethylases, Jarid1a or Phf2, contributed to the increase

in H3K4me and H4K20me3 (Table 1). H3K9me3 was reduced by the decrease in methyltransferase, SUV39H1 and 2, but not by the increase in demethylase Jmjd2c (Table 1). Because heterochromatin requires H3K9me3, HP1 α , polycomb repressive complex 2, and H3K27me3,²⁵ heterochromatin loss may be secondary to the decrease in H3K9me3 and H3K27me3.

In regard to acetylation, we found a novel aging marker of increased H4K5ac that was observed in TG and high salt-fed mice (Figure 3B and 3C). Acidosis was reported to globally hypoacetylate histones, because free acetate anions were used when monocarboxylate was effluxed via a proton extruder monocarboxylate transporter.²⁶ We thus examined chronological changes in histone acetylation of cultured cells in a low pH buffer at 37°C under 5% CO₂, and found that H4K5 was hypoacetylated acutely but hyperacetylated chronically in three kinds of cells (Figure 3D and 3E). We screened the enzyme that dominantly acetylates H4K5 using microarrays of the heart and kidney obtained from TG and high salt-fed mice. HDAC3 deacetylates histone

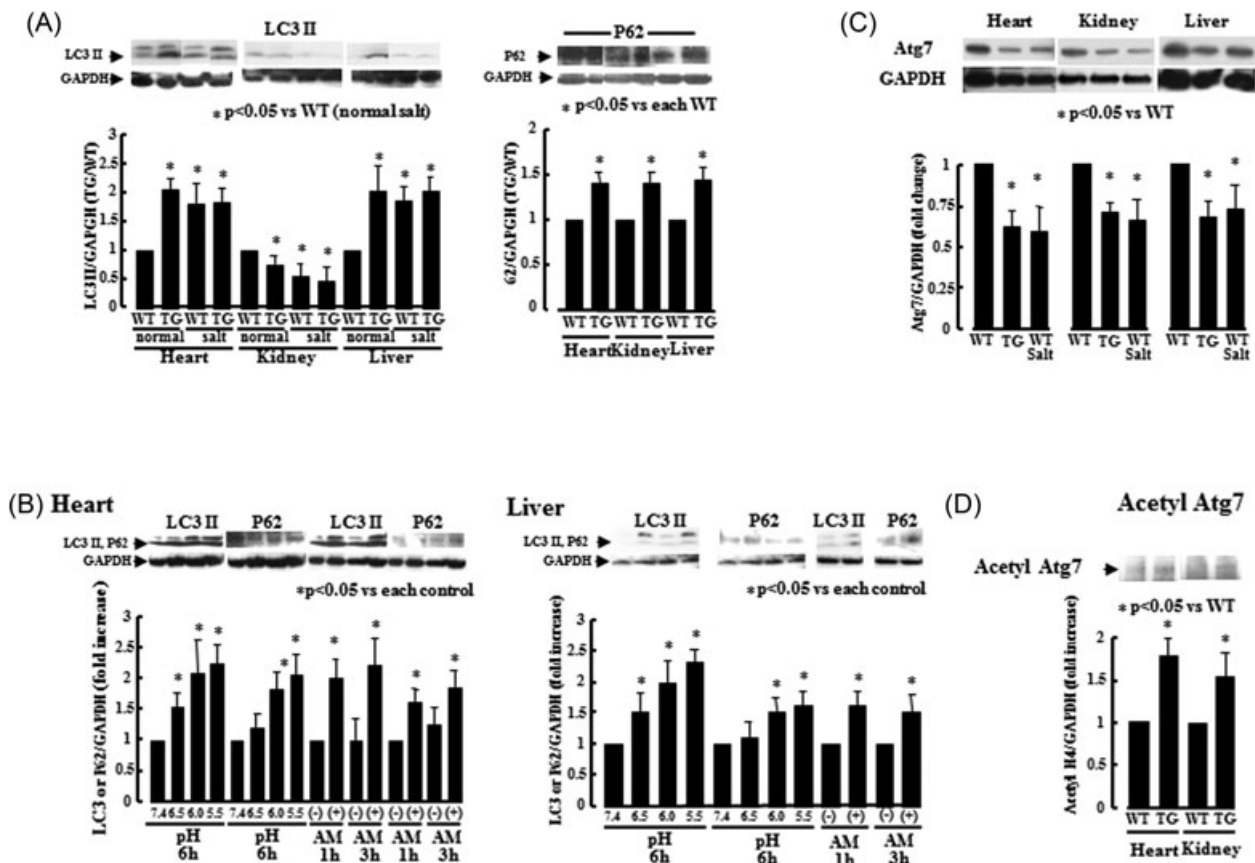


FIGURE 2 Autophagy-related proteins in coupling factor 6 (CF6) overexpressing transgenic mice (TG) and high salt-fed mice. A, LC3II in the heart, kidney, and liver obtained from normal or high salt-fed WT and TG mice (left panel) ($n = 3$ to 4) and P62 in the heart, kidney, and liver obtained from normal salt-fed WT and TG mice (right panel) ($n = 3$ to 4). B, Effect of acidosis or amiloride on LC3II and p62 in the heart and liver tissues ($n = 3$ to 4). C, Atg7 in the heart, kidney, and liver obtained from WT, TG, and high salt-fed WT mice at the age of 100 weeks ($n = 3$, respectively). D, Acetyl Atg7 in the heart and kidney

TABLE 1 Microarray data of heart and kidney from TG or high salt-fed mice

Gene ID	Gene name	TG heart	TG kidney	Salt heart	Salt kidney
Nuclear envelope					
NM_019390	lamin A	0.671 ± 0.169	0.799 ± 0.233	0.485 ± 0.069	0.591 ± 0.286
NM_010721	lamin B1	0.823 ± 0.191	0.785 ± 0.193	1.126 ± 0.500	0.596 ± 0.409
NM_010722	lamin B2	0.916 ± 0.457	0.846 ± 0.079	0.208 ± 0.072	0.221 ± 0.250
NM_007927	emerine (LEMD5)	0.997 ± 0.138	0.760 ± 0.318	0.592 ± 0.351	0.292 ± 0.232
NM_011793	BAF	0.938 ± 0.091	1.075 ± 0.280	0.995 ± 0.422	1.082 ± 0.190
NM_011605	Lap2α (TMPO, LEMD4)	0.990 ± 0.233	0.962 ± 0.175	0.500 ± 0.160	0.573 ± 0.174
21000	Lap2β (TMPO, LEMD4)	0.755 ± 0.176	0.583 ± 0.276	0.692 ± 0.005	0.000 ± 0.000
AF112300	MAN1 (LEMD3)	0.946 ± 0.298	0.730 ± 0.199	1.551 ± 0.298	0.986 ± 0.185
BC026588	LEMD2	0.798 ± 0.099	0.790 ± 0.187	0.852 ± 0.168	0.920 ± 0.502
NM_013577	SYNE1 (nesprin-1)	1.036 ± 0.273	0.841 ± 0.309	1.239 ± 0.412	1.102 ± 0.553
NM_022027	SYNE1 (nesprin-1)	0.939 ± 0.139	0.921 ± 0.105	0.627 ± 0.100	1.173 ± 0.856
BC024933	TMEM43 (LUMA)	0.907 ± 0.082	0.994 ± 0.109	0.654 ± 0.230	0.683 ± 0.261
4348	lmo7 (lim domain only 7)	0.967 ± 0.091	0.764 ± 0.265	1.207 ± 0.258	1.318 ± 0.626
12908	lmo7 (lim domain only 7)	0.935 ± 0.292	0.899 ± 0.164	1.440 ± 0.273	1.498 ± 0.337
21121	SUN1	0.910 ± 0.281	0.381 ± 0.072	0.612 ± 0.205	0.898 ± 0.374
26786	NAT10	1.051 ± 0.147	1.195 ± 0.204	0.902 ± 0.290	0.858 ± 0.519
DNA repair					
NM_007691	Checkpoint kinase 1	0.483 ± 0.097	0.677 ± 0.403	0.251 ± 0.224	0.521 ± 0.656
AF032875	Checkpoint kinase 1	0.782 ± 0.095	0.710 ± 0.373	0.704 ± 0.536	0.089 ± 0.104
NM_011233	RAD17	0.828 ± 0.060	0.895 ± 0.108	1.060 ± 0.309	0.805 ± 0.115
NM_011232	RAD1	0.941 ± 0.118	1.089 ± 0.168	0.761 ± 0.257	0.983 ± 0.379
NM_011237	RAD9	0.774 ± 0.127	0.829 ± 0.356	0.256 ± 0.087	0.399 ± 0.304
NM_008316	HUS1	1.061 ± 0.171	0.986 ± 0.260	0.702 ± 0.241	
Transcription					
NM_020493	SRF	0.850 ± 0.215	0.739 ± 0.208	0.459 ± 0.218	0.220 ± 0.099
22387	MKL1 (MAL)	0.420 ± 0.143	1.025 ± 0.106	0.625 ± 0.289	1.117 ± 0.305
9765	Btf (bclaf1b)	0.939 ± 0.219	0.636 ± 0.376	1.108 ± 0.497	0.661 ± 0.133
12636	β-Catenin	1.162 ± 0.192	1.067 ± 0.162	1.326 ± 0.320	1.261 ± 0.233
NM_021878	JARID2	1.186 ± 0.124	1.000 ± 0.214	1.084 ± 0.145	1.363 ± 0.914
12269	JARID2	0.841 ± 0.435	0.935 ± 0.191	0.433 ± 0.436	0.598 ± 0.482
DNAm					
NM_010066	Dnmt 1	0.944 ± 0.118	1.018 ± 0.105	0.873 ± 0.204	1.011 ± 0.142
NM_010067	Dnmt 2	1.008 ± 0.413	0.985 ± 0.363	0.838 ± 0.204	0.717 ± 0.571
NM_007872	Dnmt 3a	1.092 ± 0.155	0.677 ± 0.264	1.051 ± 0.425	0.718 ± 0.512
NM_010068	Dnmt 3b	0.593 ± 0.295	0.760 ± 0.118	0.676 ± 0.273	0.484 ± 0.354
NM_010931	Uhrf1	1.071 ± 0.149	1.023 ± 0.301	0.966 ± 0.505	1.027 ± 0.487
H3K4me3					
3459	Ash-2 (m2 to m3)	0.823 ± 0.031	0.948 ± 0.080	0.893 ± 0.164	1.160 ± 0.147
3859	Ash-2 (m2 to m3)	0.756 ± 0.109	0.902 ± 0.283	1.042 ± 0.270	0.910 ± 0.369
24379	MLL1	0.950 ± 0.191	0.814 ± 0.177	0.883 ± 0.319	0.443 ± 0.153
889	JARID1A (demethylase)	0.748 ± 0.515	0.627 ± 0.249	0.561 ± 0.166	0.609 ± 0.529
16146	JARID1A (demethylase)	0.521 ± 0.231	0.990 ± 0.528	0.511 ± 0.273	0.790 ± 0.200

(Continues)

TABLE 1 (Continued)

Gene ID	Gene name	TG heart	TG kidney	Salt heart	Salt kidney
H3K9me3					
NM_011514	SUV39H1	0.752 ± 0.137	0.883 ± 0.264	0.828 ± 0.264	0.842 ± 0.320
2920	SUV39H2	0.741 ± 0.196	0.764 ± 0.158	0.576 ± 0.157	0.219 ± 0.288
NM_022724	SUV39H2	0.971 ± 0.107	0.924 ± 0.035	1.492 ± 0.151	0.939 ± 0.392
AF109906	G9a (ehmt2), mono di-MT	1.065 ± 0.083	1.135 ± 0.148	0.660 ± 0.560	0.841 ± 0.531
AF109906	ehmt2, mono di-MT	1.103 ± 0.215	0.927 ± 0.102	0.786 ± 0.160	1.216 ± 0.265
NM_018877	SETDB1	0.900 ± 0.117	0.718 ± 0.138	0.978 ± 0.382	0.726 ± 0.464
X14805	DNMT-1, G9a activator	0.684 ± 0.206	0.586 ± 0.254	1.458 ± 0.659	0.783 ± 0.425
U70051	DNMT-1, G9a activator	1.023 ± 0.052	1.024 ± 0.084	0.970 ± 0.264	1.401 ± 0.553
NM_010066	DNMT-1, G9a activator	0.944 ± 0.118	1.018 ± 0.105	0.873 ± 0.204	1.011 ± 0.145
7793	Jmjd2c (demethylase)	1.109 ± 0.336	0.954 ± 0.102	1.118 ± 0.226	0.790 ± 0.305
1813	PHF8	0.952 ± 0.477	0.962 ± 0.192	1.049 ± 0.208	2.151 ± 1.313
H3K27me3					
21009	EZH2 (PRC2 complex)	1.237 ± 0.161	0.919 ± 0.155	1.308 ± 0.267	1.454 ± 0.402
NM_007971	EZH2 (PRC2 complex)	0.871 ± 0.235	0.815 ± 0.188	0.929 ± 0.371	1.342 ± 1.461
BC003922	SUZ12 (PRC2 complex)	0.940 ± 0.226	0.877 ± 0.284	0.883 ± 0.146	0.747 ± 0.168
3231	UTX (demethylase)	0.501 ± 0.081	0.829 ± 0.469	1.175 ± 0.194	0.874 ± 0.356
5000	UTX (demethylase)	1.033 ± 0.197	0.863 ± 0.309	1.224 ± 0.201	0.972 ± 0.255
8962	UTX (demethylase)	0.747 ± 0.157	0.733 ± 0.089	0.893 ± 0.295	0.500 ± 0.404
18530	JMJD3	0.691 ± 0.126	0.530 ± 0.129	0.600 ± 0.288	1.359 ± 0.629
H4K20me3					
2163	SUV420H1	0.908 ± 0.645	0.823 ± 0.167	0.955 ± 0.142	1.084 ± 0.213
4826	SUV420H1	0.820 ± 0.114	0.848 ± 0.224	1.213 ± 0.486	0.339 ± 0.581
13572	SUV420H2	1.097 ± 0.155	0.721 ± 0.429	1.130 ± 0.174	1.309 ± 0.023
19867	SUV420H2	1.020 ± 0.061	1.156 ± 0.190	0.913 ± 0.076	1.420 ± 0.089
NM_011078	phf2 (demethylase)	0.859 ± 0.087	0.765 ± 0.168	0.676 ± 0.178	0.663 ± 0.210
SPSA					
NM_007669	p21 cdkn1a	1.372 ± 0.175	1.044 ± 0.178	0.921 ± 0.151	1.005 ± 0.344
NM_009877	p16 cdkn2a	1.928 ± 0.244	1.648 ± 0.213	2.030 ± 0.559	2.939 ± 1.263
19013	IL-1 α	0.968 ± 0.052	0.779 ± 0.205	0.828 ± 0.069	0.823 ± 0.233
28757	IL-1 β	1.071 ± 0.040	0.966 ± 0.095	1.317 ± 0.202	1.240 ± 0.122
27045	IL-6	0.830 ± 0.428	0.814 ± 0.370	0.405 ± 0.350	0.582 ± 0.936
28076	CXCL1	0.998 ± 0.205	0.605 ± 0.093	1.086 ± 0.350	
763	CXCL1 (gro1)	0.441 ± 0.036	0.735 ± 0.255	0.615 ± 0.392	0.474 ± 0.784
23511	CXCL9	1.363 ± 0.190	1.819 ± 0.414	1.270 ± 0.538	
CR-related					
10833	nrf-1	0.858 ± 0.152	0.812 ± 0.158	0.151 ± 0.153	0.985 ± 0.749
NM_010938	nrf-1/skn-1	0.916 ± 0.097	0.952 ± 0.109	0.897 ± 0.195	0.840 ± 0.565
NM_020013	FGF21	0.633 ± 0.190	0.581 ± 0.199	0.462 ± 0.207	0.658 ± 0.476
NM_145953	Cystathionase	1.039 ± 0.442	0.948 ± 0.121	1.229 ± 1.136	1.226 ± 0.185
6078	CRTC1	0.988 ± 0.099	1.053 ± 0.120	1.082 ± 0.163	1.149 ± 0.361
14818	CRTC1	0.868 ± 0.354	1.028 ± 0.087	1.194 ± 0.320	0.857 ± 0.400
NM_016918	NUDT5 (NUDIX5)	0.736 ± 0.201	0.506 ± 0.105	1.155 ± 0.256	1.684 ± 1.261

(Continues)

TABLE 1 (Continued)

Gene ID	Gene name	TG heart	TG kidney	Salt heart	Salt kidney
Others					
NM_022657	FGF23	0.793 ± 0.132	0.788 ± 0.221	0.604 ± 0.076	0.738 ± 0.379
NM_013823	Klotho	1.154 ± 0.165	0.969 ± 0.070	1.150 ± 0.199	1.084 ± 0.285
NM_010206	FGFR1	1.061 ± 0.065	1.080 ± 0.167	1.442 ± 0.393	1.346 ± 0.176

lysine residues globally and H4K5 and K12 more rapidly, suggesting the dominant acetylation of H4K5. As shown in Figure 3F, HDAC3 was decreased in the heart, kidney, and liver of TG and high salt-fed mice compared with those of WT mice. Exposure of WT cells to acidosis for 24 hours also decreased HDAC3 expression without affecting other HDACs (right panel). Nuclear emerlin, an activator for HDAC3, was decreased in TG and high salt-fed mice. Taken together, it is likely that suppression of nuclear HDAC3-HDAC4-emerlin system is attributable to H4K5ac formation under chronic intracellular acidosis.

3.5 | Genomic instability and chromatin remodeling under chronic acidosis

As to genomic instability and epigenetic profile, we examined the role of sustained intracellular acidosis in nuclear architecture and chromatin remodeling in TG and high salt-fed mice. As shown in Figure 3G, the decrease in lamin A/C, emerlin, and HP1 α was confirmed in TG and high salt-fed mice. In the TG or high-salt mice heart and kidney (Table 1), neither Lap2 β that shares function and architecture with emerlin nor Sun 1 that is involved in the action of variants lamin^{27,28} was elevated, and megakaryoblastic leukaemia 1 (MKL1), a positive transcription factor for Lap2 β and Sun 1, was decreased or unchanged in TG or high-salt mice heart and kidney. Deficiencies in DNA repair mechanisms also cause genomic instability due to the accumulation of genetic damage throughout life and accelerate aging. In TG and high salt-fed mice, Chk1, a checkpoint gene in DNA damage, was downregulated in the heart and kidney (Table 1), being concomitant with partial decreases in other checkpoint genes in DNA damages such as Rad17, Rad1, Rad9, and HUS1.

4 | DISCUSSION

The major findings of this study were as follows. Both types of mice displayed shortened lifespan and early senescence-associated phenotypes such as signs of hair greying and alopecia, weight loss, and/or reduced organ mass. In these chronic intracellular acidosis mouse models, primary aging hallmarks such as impaired autophagy, epigenetic alterations, and genomic instability

were observed and may interact each other. Protein assay showed the decrease in Atg7 and an increase in nuclear acetylated LC3 II, and acetylation of Atg7 in autophagy, and the increase in H3K4me3 and H4K20me3 and the decrease in H3K9me3 and H3K27me3 and H4K5 acetylation in epigenetics, and the decrease in lamin A/C, emerlin, and HP1 α in genomic instability.

4.1 | Impact of protons on clinical outcomes and primary aging hallmarks

The excessive consumption of acid precursor foods leads to acid-base balance volatility. Chronic low-grade metabolic acidosis predisposes to metabolic imbalances such as kidney stone formation, increased bone resorption, reduced bone mineral density, and the loss of muscle mass, as well as the increased risk of chronic diseases such as type 2 diabetes, hypertension, and nonalcoholic hepatic steatosis.²⁹

The serum bicarbonate level is an independent predictor of chronic kidney disease progression. Higher serum bicarbonate levels within the normal range were associated with a reduced risk of negative outcomes in patients with chronic kidney disease, as dialysis, worsening renal function, and death.³⁰ Hypoalbuminuria and hyperkalemia were associated with low serum bicarbonate levels in chronic kidney disease patients.³¹ Furthermore, low serum bicarbonate was associated with high mortality in healthy older individuals.⁹

Both types of aging-accelerated mice displayed the decrease in Atg7, which is a key E1 like enzyme for two conjugation modifiers, Atg12 and LC, and is associated with p53-mediated cell division and apoptosis,³² in the heart and liver. In addition, LC3 II and p62 were increased in TG and high salt-fed mice, suggesting a possibility of chronic impaired autophagy. The increase in nuclear acetylated LC3 II and acetylation of Atg7 was also of characteristics in proton-induced impaired autophagy. Furthermore, both the elongation step of the isolation membrane (Atg3, 4A, 4C, 4D, 7, 12, and 16L1) and the nucleation step of the isolation membrane (Beclin1) were decreased according to data of microarray. Loss of autophagy induced by Atg7 knockdown leads to decreased levels of Chk1 and a greatly diminished ability to repair DNA double-strand breaks by homologous recombination.³³

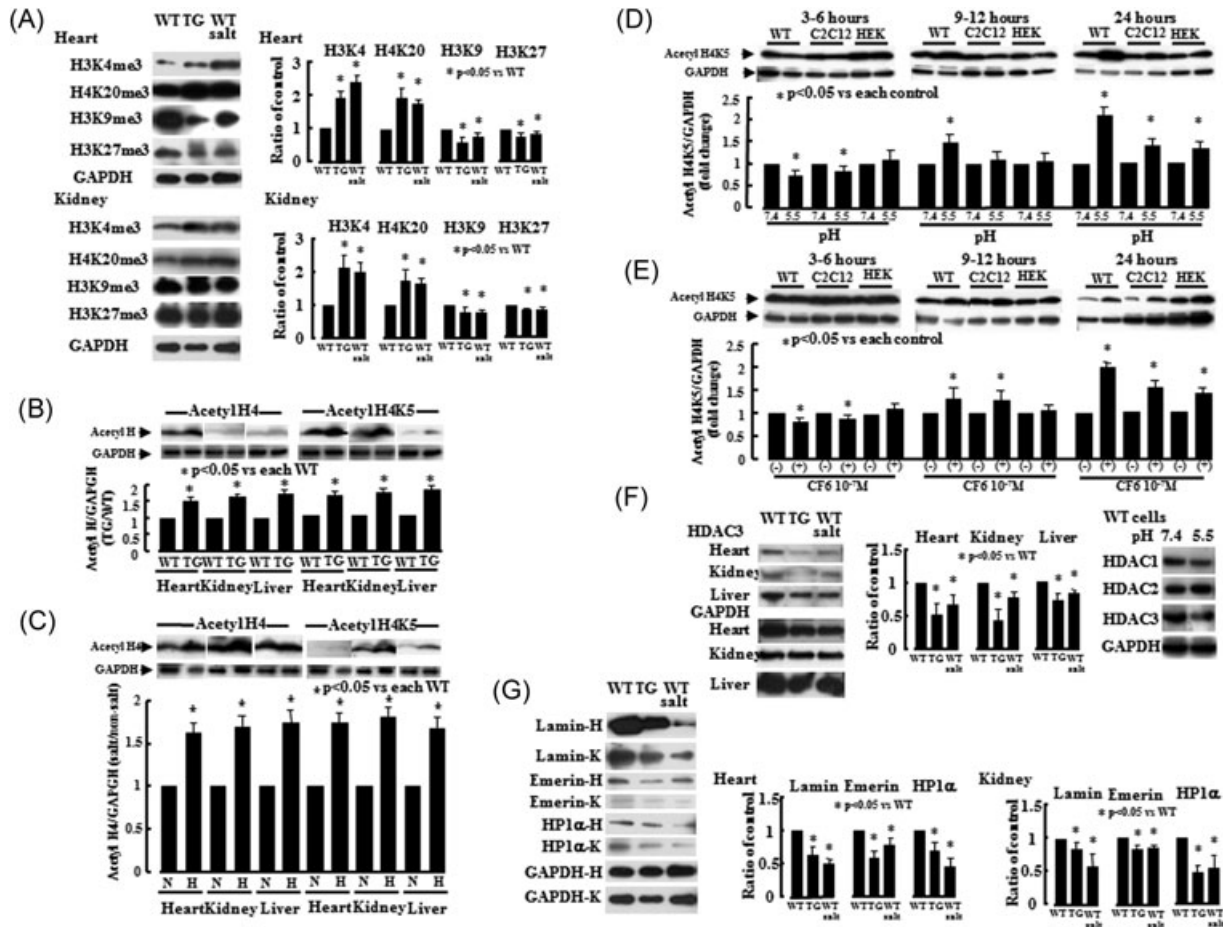


FIGURE 3 Epigenetic alterations and genomic instability in coupling factor 6 (CF6) overexpressing transgenic mice (TG) and high salt-fed mice. A, Epigenetic markers for aging of histone H4K20me3, H3K4me3, H3K9me, and H3K27me3 in WT, TG, high salt-fed WT mice at the age of 100 weeks ($n = 4$). B, Histone H4 and H4K5 acetylation (ac) in the heart, kidney, and liver obtained from WT and TG mice at the age of 100 weeks ($n = 6$, respectively). C, Histone H4 and H4K5 acetylation (ac) in the heart, kidney, and liver obtained from normal salt (N) or high salt (H)-fed WT mice ($n = 3$ to 4). D, Chronological change in H4K5ac under acidosis in WT, C2C12, and HEK 293 cells ($n = 3$, respectively). E, Chronological change in H4K5ac under CF6 at 10^{-7} M stimulation in WT, C2C12, and HEK 293 cells ($n = 3$ to 4). F, Effect of protons on histone deacetylases (HDACs) expression in the heart, kidney, and liver of WT, TG, and high salt-fed WT mice (left panel) ($n = 3$) and WT cells treated with or without acidosis (right panel). G, Nuclear architecture under sustained acidosis in WT, TG, and high salt-fed WT mice at the age of 100 weeks ($n = 3$). H, heart; K, kidney

It is of interest that the increase in H3K4me and H4K20me3 may be dependent on the decrease in histone demethylases, Jarid1a or Phf2, whereas the decrease in H3K9me3 may be caused by the decrease in methyltransferase, SUV39H1 and 2. In the current study, we found a novel aging marker of increased H4K5ac that was observed in TG and high salt-fed mice and may be characteristics of proton-induced accelerated aging. In addition, we determined its mechanisms that suppression of nuclear HDAC3-HDAC4-emerin system may be attributable to H4K5ac formation under chronic intracellular acidosis.

Genetic abnormality in nuclear lamina such as lamin and emerin causes human accelerated aging syndrome laminopathy. Genetic variants of emerin contributes to emerin-related accelerated aging laminopathy, but its phenotype was reported to be attenuated by adaptation of

elevated Lap2 β that shares the function and architecture with emerin.³⁴⁻³⁶ Genetic variants of lamin A/C, progerin, also causes another aging laminopathy, Hutchinson-Gilford progeria syndrome.³⁷ Sun 1 is reported to be involved in its aging pathogenesis,^{27,28} and progerin reduces the transcription of antioxidant genes and promotes genomic instability by suppressing the complex formation of NRF2 and SIRT6.³⁸ It should be emphasized that in our models, nuclear architecture impairment was associated with the decrease in lamin A/C, emerin, and HP1 α .

4.2 | Underlying mechanism for proton-induced accelerated aging

Expression of F₁F_o-ATP synthase has been identified in ectopic locations, together with the four complexes of

TABLE 2 Microarray data of insulin and sirtuin 6 signalling

Gene ID	Gene name	TG heart	TG kidney	Salt heart	Salt kidney
		Mean \pm SD	Mean \pm SD	Mean \pm SD	Mean \pm SD
12912 BC013345	igfbp1	1.008 \pm 0.148	1.066 \pm 0.106	1.243 \pm 0.193	1.141 \pm 0.269
636 NM_008341	igfbp1	0.476 \pm 0.162	0.574 \pm 0.304	0.578 \pm 0.194	0.505 \pm 0.236
6576 AF412811	lipin 1	0.992 \pm 0.015	1.138 \pm 0.057	1.038 \pm 0.175	0.990 \pm 0.156
10868 NM_015763	lipin 1	0.917 \pm 0.075	0.912 \pm 0.097	0.794 \pm 0.499	0.811 \pm 0.498
22555 NM_011044	pck 1	0.868 \pm 0.201	0.789 \pm 0.244	1.309 \pm 0.656	0.995 \pm 0.210
21392 NM_133232	pfkfb 3	0.805 \pm 0.351	0.721 \pm 0.312	1.155 \pm 0.458	0.986 \pm 1.198
12746 AK007410	gadd 45g	0.970 \pm 0.255	0.968 \pm 0.111	1.120 \pm 0.234	1.258 \pm 0.258
2820 NM_011817	gadd 45g	0.871 \pm 0.119	0.968 \pm 0.111	0.887 \pm 0.317	1.236 \pm 0.893
5299 NM_007606	car 3	1.013 \pm 0.127	1.167 \pm 0.064	1.183 \pm 0.178	1.109 \pm 0.130
25101 NM_026713	mogat 1	0.807 \pm 0.187	0.850 \pm 0.154	0.946 \pm 0.159	1.463 \pm 0.188
14525 NM_019650	gos 2	1.007 \pm 0.276	1.032 \pm 0.304	0.676 \pm 0.184	0.863 \pm 0.406
28757 NM_008361	il 1b	1.017 \pm 0.040	0.966 \pm 0.095	1.317 \pm 0.202	1.240 \pm 0.122
12511 NM_011704	vanin 1	1.058 \pm 0.267	0.936 \pm 0.256	0.695 \pm 0.535	1.179 \pm 0.344
220 NM_007643	cd 36	0.815 \pm 0.227	0.778 \pm 0.132	1.515 \pm 0.539	1.335 \pm 0.395
16025 AB006442	igf1r	0.733 \pm 0.100	0.796 \pm 0.123	0.743 \pm 0.207	0.912 \pm 0.155
23265 L22143	igf2r	0.978 \pm 0.249	0.897 \pm 0.173	1.167 \pm 0.170	1.153 \pm 0.281
7001 NM_010568	insr	1.031 \pm 0.133	0.928 \pm 0.249	1.408 \pm 0.360	1.571 \pm 0.489
8949 AF090738	irs2	1.263 \pm 0.319	0.825 \pm 0.147	1.100 \pm 0.227	0.785 \pm 0.262
8882 NM_009652	akt1	0.914 \pm 0.158	0.828 \pm 0.234	0.647 \pm 0.122	0.908 \pm 0.250
18835 AK010511	akt2	1.142 \pm 0.168	1.058 \pm 0.118	1.114 \pm 0.218	1.105 \pm 0.099
20683 NM_007434	akt2	1.142 \pm 0.168	0.791 \pm 0.236	1.243 \pm 0.348	1.024 \pm 0.167
20808 NM_011785	akt3	0.754 \pm 0.217	0.722 \pm 0.135	1.039 \pm 0.209	0.900 \pm 0.246
1539 \times 04480	igf1	0.923 \pm 0.081	0.820 \pm 0.234	1.017 \pm 0.264	1.127 \pm 0.439
20737 NM_010512	igf1	0.798 \pm 0.292	1.098 \pm 0.525	0.580 \pm 0.445	0.392 \pm 0.383
15164 BC013754	mapk3	0.891 \pm 0.412	0.991 \pm 0.223	0.698 \pm 0.383	0.878 \pm 0.537
17611 NM_008343	ins2igfbp3	0.890 \pm 0.311	0.720 \pm 0.056	0.954 \pm 0.310	1.297 \pm 0.461
10189 NM_008960	pten	1.135 \pm 0.272	1.320 \pm 0.327	0.754 \pm 0.123	-
17531 NM_019827	gsk3b	0.986 \pm 0.171	0.871 \pm 0.104	0.876 \pm 0.075	1.028 \pm 0.157
NM_019739	foxo1	0.930 \pm 0.066	0.970 \pm 0.071	1.044 \pm 0.319	1.048 \pm 0.374
13276 NM_007961	etv6	0.997 \pm 0.082	1.135 \pm 0.182	1.137 \pm 0.263	0.873 \pm 0.428

oxidative phosphorylation, which were identified by proteomic methods and mass spectrometry.³⁹ The whole F₁F₀-ATP synthase complex localizes on the plasma membrane in hepatocytes, and catalyzes both ATP synthesis and reverse ATP hydrolysis.⁴⁰ The plasma membrane F₁F₀ ATP synthase stimulation by apoprotein A-I triggers the endocytosis of high density lipoprotein particle.⁴¹ In endothelial cells, ATP synthesis activity is detected on the cell surface after addition of ADP and inorganic phosphate.⁴² In C6 glioma cells, the whole respiratory chain localizes on the cell surface, and is involved in ATP synthesis coupled to oxygen consumption in isolated plasma membrane.⁴³

We checked whether CF6 and high salt diet-induced intracellular acidosis accelerated aging through established pathways such as insulin/insulin-like growth factor signaling, the target of rapamycin (mTOR), and caloric restriction. We found no changes in mTOR that is a potent suppressor for antiaging Atg13,⁴⁴ no change or decrease in insulin/insulin-like growth factor signaling such as FOXO1, ETV6,^{45,46} PI3K, and AKT,^{16,46} and no change in calorie restriction-related molecules such as cystathionase and cyclic AMP responsive element (CREB)-regulated transcriptional coactivator (CRTC-1)^{47,48} (Table 1) and other several effector proteins (Table 2). Sirtuin 6 and fibroblast growth factor (FGF) 21 that are potent inhibitors of insulin signaling^{49,50} declined rather in TG and salt-fed mice (Table 1).

Nrf (NF-E2-related factor) orthologue SKN-1 that is inhibited by reduced insulin signaling and implicated in longevity,⁵¹ was unchanged in TG and salt-fed mice (Table 1), suggesting that neither TG nor high salt-fed mice displayed accelerated aging through established longevity pathways. Rather, organs obtained from TG or high salt-fed mice displayed an increase in p16 cdkn2a expression that was recently reported to influence lifespan negatively and promote age-dependent changes in several organs³ (Table 1).

In conclusion, chronic intracellular acidosis induced by circulating mitochondrial peptide or high salt intake engages in a mutually stimulatory amplification cascade of aging. The present findings will widen our understanding of aging and impaired autophagy mechanism, and provide implications in novel pharmaceutical target for antiaging therapy.

ACKNOWLEDGEMENT

This study is supported by Grant-in-Aid for Scientific Research (Nos. 19590800, 21590946, and 15K09151 for TO) from the Ministry of Education, Culture, Sports, Science and Technology, Japan.

CONFLICTS OF INTEREST

The authors declare that there are no conflicts of interest.

AUTHOR CONTRIBUTIONS

TO, MT, KI, KM (Koji M), MK, KM (Kasumi M), TT, HT, and KO contributed to designing research studies. TO, MT, KI, and KM (Koji M) contributed to conducting experiments, acquiring data, and analyzing data. TO and KO contributed to providing reagents and writing the manuscript.

ORCID

Tomohiro Osanai  <http://orcid.org/0000-0001-6364-3861>

REFERENCES

- López-Otín C, Blasco MA, Partridge L, Serrano M, Kroemer G. The hallmarks of aging. *Cell*. 2013;153:1194-1217.
- Mattison JA, Colman RJ, Beasley TM, et al. Caloric restriction improves health and survival of rhesus monkeys. *Nat Commun*. 2017;8:14063.
- Baker DJ, Childs BG, Durik M, et al. Naturally occurring p16 (Ink4a)-positive cells shorten healthy lifespan. *Nature*. 2016;530:184-189.
- Liguori I, Russo G, Curcio F, et al. Oxidative stress, aging, and diseases. *Clin Interv Aging*. 2018;13:757-772.
- Rodier F, Campisi J. Four faces of cellular senescence. *J Cell Biol*. 2011;192:547-556.
- Fagherazzi G, Vilier A, Bonnet F, et al. Dietary acid load and risk of type 2 diabetes: The E3N-EPIC cohort study. *Diabetologia*. 2014;57:313-320.
- Murakami K, Sasaki S, Takahashi Y, Uenishi K. Association between dietary acid-base load and cardiometabolic risk factors in young Japanese women. *Br J Nutr*. 2008;100:642-651.
- Buclin T, Cosma M, Appenzeller M, et al. Diet acids and alkalis influence calcium retention in bone. *Osteoporos Int*. 2001;12:493-499.
- Raphael KL, Murphy RA, Shlipak MG, et al. Health ABC Study. Bicarbonate concentration, acid-base status, and mortality in the health, aging, and body composition study. *Clin J Am Soc Nephrol*. 2016;11:308-316.
- Osanai T, Magota K, Tanaka M, et al. Intracellular signaling for vasoconstrictor coupling factor 6: novel function of β -subunit of ATP synthase as receptor. *Hypertension*. 2005;46:1140-1146.
- Izumiyama K, Osanai T, Sagara S, et al. Estrogen attenuates coupling factor 6-induced salt-sensitive hypertension and cardiac systolic dysfunction in mice. *Hypertens Res*. 2012;35:539-546.
- Kumagai A, Osanai T, Katoh C, et al. Coupling factor 6 downregulates platelet endothelial cell adhesion molecule-1 via c-Src activation and acts as a proatherogenic molecule. *Atherosclerosis*. 2008;200:45-50.
- Osanai T, Kamada T, Fujiwara N, et al. A novel inhibitory effect on prostacyclin synthesis of coupling factor 6 extracted from the heart of spontaneously hypertensive rats. *J Biol Chem*. 1998;273:31778-31783.
- Osanai T, Tanaka M, Kamada T, et al. Mitochondrial coupling factor 6 as a novel endogenous vasoconstrictor. *J Clin Invest*. 2001;108:1023-1030.
- Osanai T, Tomita H, Kushibiki M, et al. Coupling factor 6 enhances Src-mediated responsiveness to angiotensin II in resistance arterioles and cells. *Cardiovasc Res*. 2009;81:780-787.
- Osanai T, Tanaka M, Magota K, Tomita H, Okumura K. Coupling factor 6-induced activation of ecto-F1Fo complex induces insulin resistance, mild glucose intolerance and elevated blood pressure in mice. *Diabetologia*. 2012;55:520-529.
- Tanaka M, Osanai T, Murakami R, et al. Effect of vasoconstrictor coupling factor 6 on gene expression profile in human vascular endothelial cells: enhanced release of asymmetric dimethylarginine. *J Hypertens*. 2006;24:489-497.
- Li XL, Xing QC, Dong B, et al. Plasma level of mitochondrial coupling factor 6 increases in patients with type 2 diabetes mellitus. *Int J Cardiol*. 2007;117:411-412.
- Osanai T, Nakamura M, Sasaki S, et al. Plasma concentration of coupling factor 6 and cardiovascular events in patients with end-stage renal disease. *Kidney Int*. 2003;64:2291-2297.
- Osanai T, Sasaki S, Kamada T, et al. Circulating coupling factor 6 in human hypertension: role of reactive oxygen species. *J Hypertens*. 2003;21:2323-2328.
- Osanai T, Fujiwara N, Sasaki S, et al. Novel pro-atherogenic molecule coupling factor 6 is elevated in patients with stroke: a possible linkage to homocysteine. *Ann Med*. 2010;42:79-86.
- Osanai T, Okada S, Sirato K, et al. Mitochondrial coupling factor 6 is present on the surface of human vascular endothelial cells and released by shear stress. *Circulation*. 2001;104:3132-3136.

23. Cheng XJ, Fisone G, Aizman O, et al. PKA-mediated phosphorylation and inhibition of Na(+)-K(+)-ATPase in response to beta-adrenergic hormone. *Am J Physiol*. 1997;273:C893-C901.
24. Greer EL, Maures TJ, Hauswirth AG, et al. Members of the H3K4 trimethylation complex regulate lifespan in a germline-dependent manner in *C. elegans*. *Nature*. 2010;466:383-387.
25. Boros J, Arnoult N, Stroobant V, Collet JF, Decottignies A. Polycomb repressive complex 2 and H3K27me3 cooperate with H3K9 methylation to maintain heterochromatin protein 1 α at chromatin. *Mol Cell Biol*. 2014;34:3662-3674.
26. McBrien MA, Behbahan IS, Ferrari R, et al. Histone acetylation regulates intracellular pH. *Mol Cell*. 2013;49:310-321.
27. Cau P, Navarro C, Harhour K, et al. Nuclear matrix, nuclear envelope and premature aging syndromes in a translational research perspective. *Semin Cell Dev Biol*. 2014;29C:125-147.
28. Chen CY, Chi YH, Mutalif RA, et al. Accumulation of the inner nuclear envelope protein Sun1 is pathogenic in progeric and dystrophic laminopathies. *Cell*. 2012;149:565-577.
29. Carnauba R, Baptistella A, Paschoal V, Hübscher G. Diet-induced low-grade metabolic acidosis and clinical outcomes: a review. *Nutrients*. 2017;9:538. <https://doi.org/10.3390/nu9060538>.
30. Raphael KL, Wei G, Baird BC, Greene T, Beddhu S. Higher serum bicarbonate levels within the normal range are associated with better survival and renal outcomes in African Americans. *Kidney Int*. 2011;79:356-362.
31. Kanda E, Ai M, Kuriyama R, Yoshida M, Shiigai T. Dietary acid intake and kidney disease progression in the elderly. *Am J Nephrol*. 2014;39:145-152.
32. Lee IH, Kawai Y, Fergusson MM, et al. Atg7 modulates p53 activity to regulate cell cycle and survival during metabolic stress. *Science*. 2012;336:225-228.
33. Liu EY, Xu N, O'Prey J, et al. Loss of autophagy causes a synthetic lethal deficiency in DNA repair. *Proc Natl Acad Sci USA*. 2015;112:773-778.
34. Bakay M, Wang Z, Melcon G, et al. Nuclear envelope dystrophies show a transcriptional fingerprint suggesting disruption of Rb-MyoD pathways in muscle regeneration. *Brain*. 2006;129:996-1013.
35. Melcon G, Kozlov S, Cutler DA, et al. Loss of emerin at the nuclear envelope disrupts the Rb1/E2F and MyoD pathways during muscle regeneration. *Hum Mol Genet*. 2006;15:637-651.
36. Ozawa R, Hayashi YK, Ogawa M, et al. Emerin-lacking mice show minimal motor and cardiac dysfunctions with nuclear-associated vacuoles. *Am J Pathol*. 2006;168:907-917.
37. Schreiber KH, Kennedy BK. When lamins go bad: nuclear structure and disease. *Cell*. 2013;152:1365-1375.
38. Kubben N, Zhang W, Wang L, et al. Repression of the antioxidant NRF2 pathway in premature aging. *Cell*. 2016;165:1361-1374.
39. Panfoli I, Ravera S, Bruschi M, Candiano G, Morelli A. Proteomics unravels the exportability of mitochondrial respiratory chains. *Expert Rev Proteomics*. 2011;8:231-239.
40. Mangiullo R, Gnoni A, Leone A, Gnoni GV, Papa S, Zanotti F. Structural and functional characterization of F₀F₁-ATP synthase on the extracellular surface of rat hepatocytes. *Biochim Biophys Acta*. 2008;1777:1326-1335.
41. Martinez LO, Jacquet S, Esteve JP, et al. Ectopic β -chain of ATP synthase is an apolipoprotein A-I receptor in hepatic HDL endocytosis. *Nature*. 2003;421:75-79.
42. Arakaki N, Nagao T, Niki R, et al. Possible role of cell surface H⁺-ATP synthase in the extracellular ATP synthesis and proliferation of human umbilical vein endothelial cells. *Mol Cancer Res*. 2003;1:931-939.
43. Ravera S, Aluigi MG, Calzia D, Ramoino P, Morelli A, Panfoli I. Evidence for ectopic aerobic ATP production on C6 glioma cell plasma membrane. *Cell Mol Neurobiol*. 2011;31:313-321.
44. Madeo F, Tavernarakis N, Kroemer G. Can autophagy promote longevity? *Nat Cell Biol*. 2010;12:842-846.
45. Alic N, Giannakou ME, Papatheodorou I, et al. Interplay of dFOXO and two ETS-family transcription factors determines lifespan in *Drosophila melanogaster*. *PLoS Genet*. 2014;10:e1004619-1146.
46. Sagara S, Osanai T, Itoh T, et al. Overexpression of coupling factor 6 attenuates exercise-induced physiological cardiac hypertrophy by inhibiting PI3K/Akt signaling in mice. *J Hypertens*. 2012;30:778-786.
47. Hine C, Harputlugil E, Zhang Y, et al. Endogenous hydrogen sulfide production is essential for dietary restriction benefits. *Cell*. 2015;160:132-144.
48. Burkewitz K, Morante I, Weir HJM, et al. Neuronal CRTG-1 governs systemic mitochondrial metabolism and lifespan via a catecholamine signal. *Cell*. 2015;160:842-855.
49. Kanfi Y, Naiman S, Amir G, et al. The sirtuin SIRT6 regulates lifespan in male mice. *Nature*. 2012;483:218-221.
50. Zhang Y, Xie Y, Berglund ED, et al. The starvation hormone, fibroblast growth factor-21, extends lifespan in mice. *eLife*. 2012;1:e00065.
51. Robida-Stubbs S, Glover-Cutter K, Lamming DW, et al. TOR signaling and rapamycin influence longevity by regulating SKN-1/Nrf and DAF-16/FoxO. *Cell Metab*. 2012;15:713-724.

SUPPORTING INFORMATION

Additional supporting information may be found online in the Supporting Information section at the end of the article.

How to cite this article: Osanai T, Tanaka M, Izumiyama K, et al. Intracellular protons accelerate aging and switch on aging hallmarks in mice. *J Cell Biochem*. 2018;1-13.

<https://doi.org/10.1002/jcb.27302>